

Flexible Communication Avoiding Matrix Multiplication on FPGA with High-Level Synthesis

Johannes de Fine Licht
ETH Zurich
definelicht@inf.ethz.ch

Grzegorz Kwasniewski
ETH Zurich
gkwasnie@inf.ethz.ch

Torsten Hoefler
ETH Zurich
htor@inf.ethz.ch

ABSTRACT

Data movement is the dominating factor affecting performance and energy in modern computing systems. Consequently, many algorithms have been developed to minimize the number of I/O operations for common computing patterns. Matrix multiplication is no exception, and lower bounds have been proven and implemented both for shared and distributed memory systems. Reconfigurable hardware platforms are a lucrative target for I/O minimizing algorithms, as they offer full control of memory accesses to the programmer. While bounds developed in the context of fixed architectures still apply to these platforms, the spatially distributed nature of their computational and memory resources requires a decentralized approach to optimize algorithms for maximum hardware utilization. We present a model to optimize matrix multiplication for FPGA platforms, simultaneously targeting maximum performance and minimum off-chip data movement, within constraints set by the hardware. We map the model to a concrete architecture using a high-level synthesis tool, maintaining a high level of abstraction, allowing us to support arbitrary data types, and enables maintainability and portability across FPGA devices. Kernels generated from our architecture are shown to offer competitive performance in practice, scaling with both compute and memory resources. We offer our design as an open source project¹ to encourage the open development of linear algebra and I/O minimizing algorithms on reconfigurable hardware platforms.

1 INTRODUCTION

The increasing technological gap between computation and memory speeds [33] pushes both academia [1, 11, 28, 29] and industry [2, 18] to develop algorithms and techniques to minimize data movement. The first works proving I/O lower bounds for specific algorithms, e.g., Matrix Matrix Multiplication (MMM), date back to the 80s [21]. The results were later extended to parallel and distributed machines [20]. Since then, many I/O minimizing algorithms were developed for linear algebra [3, 14, 29], neural networks [10], and general programs that access arrays [6]. Minimizing I/O impacts not only performance, but also reduces bandwidth usage in a shared system. MMM is typically used as a component of larger applications [9, 31], where it co-exists with other algorithms, e.g., memory bound linear algebra operations such as matrix-vector/vector-vector operations, which benefit from a larger share of the bandwidth, but do not require large amounts of compute resources.

FPGAs are an excellent platform for accurately modeling performance and I/O to guide algorithm implementations. In contrast to software implementations, the replacement of cache with explicit on-chip memory, and isolation of the instantiated architecture,

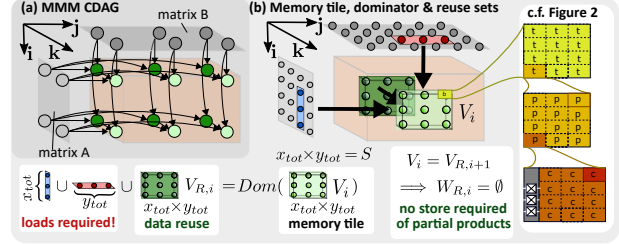


Figure 1: (a) MMM CDAG, and (b) subcomputation V_i .

yields fully deterministic behavior in the circuit: accessing memory, both on-chip and off-chip, is always done explicitly, rather than by a cache replacement scheme fixed by the hardware. The models established so far, however, pose a challenge for their applicability on FPGAs. They often rely on abstracting away many hardware details, assuming several idealized processing units with local memory and all-to-all communication [1, 20, 21, 29]. Those assumptions do not hold for FPGAs, where the physical area size of custom-designed processing elements (PEs) and their layout are among most important concerns in designing efficient FPGA implementations [25]. Therefore, performance modeling for reconfigurable architectures requires taking constraints like logic resources, fan-out, routing, and on-chip memory characteristics into account.

With an ever-increasing diversity in available hardware platforms, and as low-precision arithmetic and exotic data types are becoming key in modern DNN [4] and linear solver [17] applications, extensibility and flexibility of hardware architectures will be crucial to stay competitive. Existing high-performance FPGA implementations [22, 27] are implemented in hardware description languages (HDLs), which drastically constrains their maintenance, reuse, generalizability, and portability. Furthermore, the source code is not disclosed, such that third-party users cannot benefit from the kernel or build on the architecture.

In this work, we address all the above issues. We present a high-performance, communication avoiding MMM algorithm, which is based on both computational complexity theory [21] (Section 3.2), and on detailed knowledge of FPGA-specific features (Section 4). Our architecture is implemented in pure C++ with a small and readable code base, and to the best of our knowledge, is the first open source, high-performance MMM FPGA code. We do not assume the target hardware, and allow easy configuration of platform, degree of parallelism, buffering, data types, and matrix sizes, allowing kernels to be specialized to the desired scenario. The contributions of this paper are:

- We model a decomposition for matrix multiplication that simultaneously targets maximum performance and minimum off-chip data movement, in terms of hardware constants.

¹https://github.com/spcl/gemm_hls (10.5281/zenodo.3559536)

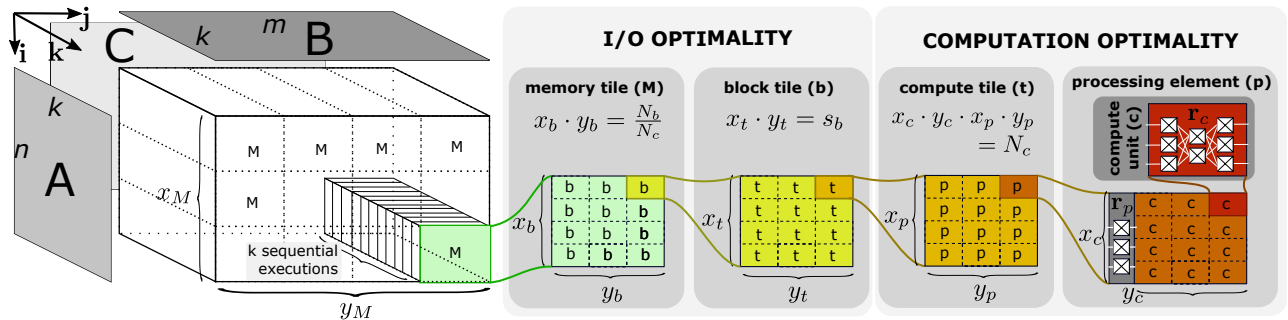


Figure 2: Decomposition of MMM achieving both performance and I/O optimality in terms of hardware resources.

- We design a mapping that allows the proposed scheme to be implemented in hardware, using the model parameters to lay out the architecture.
- We provide a plug-and-play, open source implementation of the hardware architecture in pure HLS C++, enabling portability across FPGA and demonstrating low code complexity.
- We include benchmarks for a wide range of floating point and integer types, and show the effect of adjusting parallelism and buffer space in the design, demonstrating the design’s flexibility and scalability.

2 OPTIMIZATION GOALS

In this section we introduce *what* we optimize. In Sections 3.2, 3.3, and 4 we describe *how* this is achieved. We consider optimizing the schedule of a *classical* MMM algorithm, that is, given a problem of finding C , where $C = AB$, $A \in \mathbb{R}^{m \times k}$, $B \in \mathbb{R}^{k \times n}$, $C \in \mathbb{R}^{m \times n}$, an algorithm performs $F = mnk$ multiplications and additions (pseudocode shown in Lst. 1). We therefore exclude Strassen-like routines [30] from our analysis, as the classical algorithms often perform better on practical problems and hardware [7]. We require that the optimal schedule: (1) achieves *highest performance* (takes least time-to-solution time), while (2) performing the *least number of I/O operations*, by (3) *making most efficient use of resources*.

```

1 for (i = 0; i < M; i++)
2   for (j = 0; j < N; j++)
3     for (k = 0; k < K; k++)
4       C[i, j] = C[i, j] + A[i, k]*B[k, j];

```

Listing 1: Classical MMM algorithm.

Computation On general purpose CPUs, as well as on modern GPUs, optimizing for computation is often a straightforward task. Exploiting techniques like vectorization or data alignment [34] can mostly be offloaded to compilers. Thus, most of the effort is spent on I/O minimization. When targeting FPGAs, designing an architecture that can optimally exploit available logic, even for computationally simple algorithms such as matrix multiplication, requires significant engineering effort. We must thus maintain a decomposition that is efficiently implementable in hardware, while achieving the desired theoretical properties.

I/O Schedule optimization on a parallel machine determines both the domain decomposition (which computations are assigned to

which compute units), and sequential execution (the order in which each compute unit executes its tasks). The former impacts communication between compute units (a.k.a. *horizontal I/O*), and the latter is responsible for the communication between a compute unit and a main memory (a.k.a. *a vertical I/O*). Both aspects of the parallel schedule are constrained by available resources and their interdependencies (e.g., NUMA domains or limited fan-out on FPGAs).

Resources When targeting a high utilization design on FPGA, it is critical to maintain characteristics that aid the routing process. Routing reacts poorly to large fan-in or fan-out, which typically occurs when these are dependent on the degree of parallelism: that is, if N determines the degree of parallelism in the program, 1-to- N and N -to-1 connections in the architecture should be avoided. This is true both on the granularity of individual logic units, and on the granularity of coarse-grained modules instantiated by the programmer. To accommodate this, we can regulate the size of PEs, and favor PE topologies that are easily mapped to a plane, such as grids or chains. Furthermore, mapping of a hardware architecture to the chip logic and interconnect (placement and routing) may reduce the clock frequency due to long routing paths. Due to the intractable size of the configuration space, this cannot be efficiently modeled and requires empirical evaluation of designs. The routing challenges are exasperated in FPGA chips that consist of multiple “chipllets”, such as the Xilinx UltraScale+ VU9P chip used in this paper, which hosts three “super-logical regions” (SLRs). Crossing the chipllets consumes highly limited routing resources and carries a higher timing penalty. Limiting these crossings is thus key to scaling up resource utilization.

Throughout this paper, we use the two-level notation for naming parameters (Table 1). Most of the parameter names are in the form of α_β , where α refers to some quantity, such as the total number of objects, and β determines what is the object of interest. E.g., N_c, N_b, s_b are: total number of (N) compute units (c), memory blocks (b), and a size of each memory block (s), respectively.

The target hardware contains d types of different logic resources. This typically consists of general purpose logic, such as *lookup tables* (LUTs), and more specialized arithmetic units, such as *digital signal processing units* (DSPs). We represent a quantity of these resources as a vector $\mathbf{r}_{\max} = [r_{1,\max}, \dots, r_{d,\max}]$. As a basic logical entity, we consider a “compute unit”, which is a basic circuit able to perform a single multiply-addition operation in a single cycle. Each unit is

MMM	i, j, k	Unit vectors spanning 3D iteration space.
	m, n, k	Matrix sizes in $i, j,$ and k dimensions, respectively.
	A, B	Input matrices $A \in \mathbb{R}^{m \times k}$ and $B \in \mathbb{R}^{k \times n}$.
	$C = AB$	Output matrix $C \in \mathbb{R}^{m \times n}$.
naming	α_β	Parameter naming convention. α is some quantity (i.e., size or number of objects), β is an object that α refers to.
	$\alpha_{\beta, \max}$	Hardware limit on a parameter α_β .
	$\alpha_{\text{tot}} = \prod_\beta \alpha_\beta$	The product of all tile sizes.
α	N	Total number of objects.
	x, y	Number of objects in i (or j) dimension in the enveloping tile.
	s	Intrinsic size of an object.
	w	Bit width of object (e.g., of port or data type).
	r	Vector of logic resources.
β	c	Compute units in a processing element.
	p	Processing elements in a compute tile.
	t	Compute tiles in a block tile.
	b	Block tiles in a memory tile.
optimization	$S = N_b \cdot s_b$	Total size of available on-chip memory.
	$N_c \leq N_{c, \max}$	Total number of compute units.
	Q	Total number of off-chip memory transfers.
	$\bar{F} = n \cdot m \cdot k$	Total number of multiply-addition operations required to perform MMM.
	$f \leq f_{\max}$	Achieved and maximum design frequency.
	$T = \frac{\bar{F}}{f \cdot N_c}$	Design total execution time.

Table 1: The most important symbols used in this paper.

implemented on the target hardware using some combination of logic resources r_c . Depending on the numerical precision, different number of computation resources r_c are needed to form a single compute unit, so the maximum number of compute units that can be instantiated, N_c , may vary. The compute units are organized into N_p *processing elements* (PEs), which encapsulate a closed logical task (e.g., a vector operation) of $x_c \cdot y_c$ compute units. Each PE additionally consumes r_p logic resources as orchestration overhead. This gives us the following constraint, which enforces that the total amount of resources consumed by compute units and their encompassing PEs should not exceed the total resources available:

$$\forall_{1 \leq i \leq d} N_c r_{i,c} + N_p r_{i,p} \leq r_{i, \max}, \quad (1)$$

or equivalently $\forall_{1 \leq i \leq d} N_p (r_{i,p} + r_{i,c} \cdot x_c y_c) \leq r_{i, \max}$

where d is the dimensionality of the resource vector (illustrated in the top-right side of Fig. 2).

3 OPTIMIZATION MODELS

3.1 Computation Model

To optimize computational performance we minimize the total execution runtime, which is a function of achieved parallelism (total number of compute units N_c) and the design clock frequency f . The computational logic is organized into N_p PEs, and we assume that every PE holds $x_c \cdot y_c$ compute units in dimensions x and y (see Tab. 1 for an overview of all symbols used). We model the factor N_c directly in the design, and rely on empirically fixing f , which is limited by the maximum size of data buses between PEs (i.e., $x_c w_c \leq w_{p, \max}$ and $y_c w_c \leq w_{p, \max}$, where $w_{p, \max}$ depends on the architecture, and typically takes values up to 512 bit). Formally, we can write the computational optimization problem as follows:

$$\text{minimize } T = \frac{\bar{F}}{f \cdot N_c} = \frac{mnk}{f \cdot N_p \cdot x_c y_c}$$

subject to:

$$\begin{aligned} \forall_{1 \leq i \leq d} N_p (r_{i,p} + r_{i,c} \cdot x_c \cdot y_c) &\leq r_{i, \max} \\ x_c w_c &\leq w_{p, \max} \\ y_c w_c &\leq w_{p, \max} \\ f &\leq f_{\max} \end{aligned} \quad (2)$$

That is, the time to completion T is minimized when $f \cdot N_c$ is maximized, where the number of parallel compute units N_c is constrained by the available logic resources r_{\max} of the design (this can be the full hardware chip, or any desired subset resource budget). We respect routing constraints by observing a maximum bus width $w_{p, \max}$, and must stay within the target frequency f_{\max} .

3.2 I/O Model

3.2.1 State-of-the-art of Modeling I/O for MMM.

Minimizing the I/O cost is essential for achieving high performance on modern architectures, even for traditionally compute-bound kernels like MMM [24]. In this section, we sketch a theoretical background from previous works which lays foundation for our FPGA model. Following the state-of-the-art I/O models [19, 21, 29] we assume that a parallel machine consists of p processors, each equipped with a fast private memory of size S words. To perform an arithmetic operation, processor p_i is required to have all operands in its fast memory. The principal idea behind the I/O optimal schedule is to maximize the *computational intensity*, i.e., the number of arithmetic operations performed per one I/O operation. This naturally expresses the notion of data reuse, which reduces both vertical (through memory hierarchy) and horizontal (between compute units) I/O (Section 2).

Algorithm as a Graph We represent an entire execution of an algorithm as a *computation directed acyclic graph* (CDAG) [5, 21, 24] $G = (V, E)$, where every vertex $v \in V$ corresponds to some unique value during the execution, and edges $e \in E$ represent data dependencies between them. Vertices without incoming edges are *inputs*, and the ones without outgoing edges are *outputs*. The remaining vertices are intermediate results. In the context of MMM, matrices A and B form $m \times k$ and $k \times n$ input vertices, respectively, and partial sums of C form mnk intermediate vertices, with inputs both from corresponding vertices of A and B , and previous partial sums of C . The output vertices are formed by the $m \times n$ vertices of C which represent the last of k partial sums. The MMM CDAG is shown in Fig. 1a.

I/O as Graph Pebbling Hong and Kung [21] introduced the red-blue pebble game abstraction to model the I/O cost of a sequential schedule on a CDAG. We refer a reader to the original paper for the formal definition and details of this game: here we just draw its simplistic sketch. The key idea is to play a pebbling game with a limited number of red pebbles (corresponding to the small-but-fast memory) and an unlimited number of blue pebbles (large, slow memory). The rules are that one can put a red pebble on a vertex only if all its direct predecessors also have red pebbles (which represent computing a value, while all operands are in the fast memory). Placing a blue pebble on a red one corresponds to a store

operation, and putting a red pebble on a blue corresponds to a load. Initially, only input vertices have blue pebbles on them. The goal is to put blue pebbles on the output vertices. In this model, the I/O optimal schedule is a sequence of pebbling moves which minimizes the load and store operations.

Schedule as a Graph Partition In our work, we extend the methodology and results of COSMA [24], which is based on the red-blue pebble game. We partition the CDAG $G = (V, E)$ into h disjoint subsets (a.k.a. *subcomputations*) $V_i, i = 1 \dots h, V_i \subset V$, such that each V_i has a constant number X of input and output vertices (which form the *Dominator set* and *Minimum set*, respectively). The collection of all $\{V_i\}, \cup V_i = V$ is called an X -partition of G . The authors show that an I/O optimal scheme can be derived from finding an X -partition $\{V_i\}$ of a smallest cardinality, for some value of X . We will use this result to build our model.

Optimal Graph Partition as Maximizing Computational Intensity In COSMA [24], it is shown that the I/O optimal MMM schedule maximizes the *computational intensity* of each subcomputation V_i , that is, the number of arithmetic operations per I/O operation. Formally:

$$\begin{aligned} & \text{maximize } \frac{|V_i|}{|\text{Dom}(V_i)| - |V_{R,i}| + |W_{B,i}|} \\ & \text{subject to: } |V_{R,i}| \leq S, \end{aligned} \quad (3)$$

where $|V_i|$ is a number of values updated in subcomputation V_i , $|\text{Dom}(V_i)|$ is the number of inputs of V_i (the *Dominator set*), $|V_{R,i}|$ is the number of inputs that are already in the on-chip memory (data reuse), and $|W_{B,i}|$ is the number of partial results that have to be stored back to off-chip memory. Therefore, we aim to maximize utilization of all available on-chip memory, to increase the reuse of data $|V_{R,i}|$ that is already loaded. The sets V_i , $\text{Dom}(V_i)$, and $V_{R,i}$ are depicted in Fig. 1b.

3.2.2 Extending to the FPGA Scenario.

I/O Optimal Schedule vs. FPGA Constraints State-of-the-art I/O models [19, 21, 29] assume that a parallel machine consists of p processors, each equipped with a small private memory of constant size S words (two-level memory model). Under these assumptions, COSMA establishes that the I/O optimal MMM schedule is composed of $h = mnk/S$ subcomputations, each performing S multiply-addition operations while loading $2\sqrt{S}$ elements from matrices A and B . However, in the FPGA setting these assumptions do not hold, as the number of compute units N_c is a variable depending on both hardware resources (which is constant), and on the processing element design. Furthermore, the mapping between processing elements and available BRAM blocks is also constrained by ports and limited fan-out. We impose the additional requirement that compute and memory resources must be equally distributed among PEs, posing additional restrictions on a number of available resources and their distribution for each subcomputation V_i to secure maximum arithmetic throughput and routing feasibility:

- (1) The number of parallel compute units N_c is maximized.
- (2) The work is load balanced, such that each compute unit performs the same number of computations.
- (3) Each memory block is routed to only one compute unit (i.e., they are not shared between compute units).

- (4) Each processing element p performs the same logical task, and consumes the same amount of computational and memory block resources.

Memory resources To model the memory resources of the FPGA, we consider the bit-length of w_c , depending on the target precision. The machine contains N_b on-chip memory blocks, each capable of holding s_b words of the target data type, yielding a maximum of

$$S = N_b \cdot s_b$$

words that can be held in on-chip memory. s_b takes different values depending on w_c (e.g., 16 bit for half precision floating point, or a 64 bit long unsigned integer). Each memory block supports one read and one write of up to w_b bits in a single cycle in a pipelined fashion.

FPGA-constrained I/O Minimization We denote each V_i as a *memory tile* M , as its size in i and j dimensions determines the memory reuse. To support a hierarchical hardware design, each M is further decomposed into several levels of tiling. This decomposition encapsulates hardware features of the chip, and imposes several restrictions on the final shape of M . The tiling scheme is illustrated in Fig. 2. We will cover the purpose and definition of each layer in the hierarchy shortly in Sec. 3.3, but for now use that the dimensions of the full memory tile M are:

$$\begin{aligned} x_{\text{tot}} &= x_c \cdot x_p \cdot x_t \cdot x_b \\ y_{\text{tot}} &= y_c \cdot y_p \cdot y_t \cdot y_b, \end{aligned} \quad (4)$$

and we set $|V_i| = x_{\text{tot}}y_{\text{tot}}$. Following the result from [24], a schedule that minimizes the number I/O operations, loads x_{tot} elements of one column of matrix A , y_{tot} elements of one row of matrix B and reuses $x_{\text{tot}}y_{\text{tot}}$ previous partial results of C , thus computing an outer product of the loaded row and column. We now rewrite Eq. 3 as:

$$\begin{aligned} & \text{maximize } \frac{x_{\text{tot}}y_{\text{tot}}}{x_{\text{tot}} + y_{\text{tot}}} \\ & \text{subject to: } x_{\text{tot}} + y_{\text{tot}} \leq S \\ & \quad x_{\text{tot}}y_{\text{tot}} \leq S, \end{aligned} \quad (5)$$

and the total number of I/O operations as:

$$Q = mn \left(1 + k \left(\frac{1}{x_{\text{tot}}} + \frac{1}{y_{\text{tot}}} \right) \right). \quad (6)$$

This expression is minimized when:

$$x_{\text{tot}} = y_{\text{tot}} = \sqrt{S} \quad (7)$$

That is, a memory tile is a square of size S . Eq. 6 therefore gives us a theoretical lower bound on $Q \leq 2mnk/\sqrt{S}$, assuming that all available memory can be used effectively. However, the assumptions stated in Sec. 3.2 constrain the perfect distribution of hardware resources, which we model in Sec. 3.3.

3.3 Resource Model

Based on the I/O model and the FPGA constraints, we create a logical hierarchy which encapsulates various hardware resources, which will guide the implementation to maximize I/O and performance. We assume a chip contains $\mathbf{r}_{\text{max}} = \{r_{1,\text{max}}, \dots, r_{t,\text{max}}\}$ different hardware resources (see Sec. 2). The dimensionality and length of a vector depends on the target hardware – e.g., Intel Arria 10 and Stratix 10 devices expose native floating point DSPs,

```

1 // Memory tiles m
2 for (im = 1; im ≤ n; im = im + xtot)
3   for (jm = 1; jm ≤ m; jm = jm + ytot)
4     for (k = 1; k ≤ k; k = k + 1) // Full dimension k
5 // [Sequential] Block tiles b in memory tile
6   for (ib = im; ib ≤ im + xtot; im = im + xt xc xp)
7     for (jb = jm; jb ≤ jm + ytot; jm = jm + yt yp yc)
8 // [Sequential] Compute tiles t in block tile
9   for (it = ib; it ≤ ib + xt xp xc; ib = ib + xc xp)
10  for (jt = yb; jt ≤ jb + yt yp yc; jt = jt + yc yp)
11 // [Parallel] Processing elements p in compute tile
12  forall (ip = it; ip ≤ it + xp xc; it = it + xc)
13  forall (jp = jt; jp ≤ jt + yp yc; jp = jp + yc)
14 // [Parallel] Compute units c in processing element
15  forall (ic = ip; ic ≤ ip + xc; ic = ic + 1)
16  forall (jc = jp; jc ≤ jp + yc; jc = jc + 1)
17    C(ic, jc) = C(ic, jc) + A(ic, k) · B(k, jc)

```

Listing 2: Pseudocode of the tiled MMM algorithm.

each implementing a single operation, whereas a Xilinx UltraScale+ device requires a combination of logic resources. We model fast memory resources separately as memory blocks (e.g., M20K blocks on Intel Stratix 10, or Xilinx BRAM units). We consider a chip contains N_b memory blocks, where each unit can store s_b elements of the target data type and has a read/write port width of w_b bits. The scheme is organized as follows (shown in Fig. 2):

- (1) A compute unit c consumes r_c hardware resources, and can throughput a single multiplication and addition per cycle. Their maximal number

$$N_{c,\max} \leq \min_{1 \leq i \leq t} \left(\frac{r_{i,\max}}{r_{i,c}} \right)$$

for a given numerical precision is a hardware constant, given by the available resources r_{\max} .

- (2) A processing element p encapsulates $x_c \cdot y_c$ compute units. Each processing element requires additional r_p resources for overhead logic.
- (3) A compute tile t encapsulates $x_p \cdot y_p$ processing elements. One compute tile contains all available compute units $x_c \cdot y_c \cdot x_p \cdot y_p = N_c$.
- (4) A block tile b encapsulates $x_t \cdot y_t = s_b$ compute tiles, filling the entire internal capacity s_b of currently allocated memory blocks.
- (5) A memory tile M encapsulates $x_b \cdot y_b = \left\lfloor \frac{N_b}{N_{b,\min}} \right\rfloor$ block tiles (discussed below), using all available N_b memory blocks.

Pseudocode showing the *iteration space* of this decomposition is shown in Lst. 2, consisting of 11 nested loops. Each loop is either a *sequential* for-loop, meaning that no iterations will overlap, and will thus correspond to *pipelined* loops in the HLS code; or a *parallel* forall-loop, meaning that every iteration is executed every cycle, corresponding to *unrolled* loops in the HLS code. We require that the sequential loops are coalesced into a single pipeline, such that no overhead is paid at iterations of the outer loops.

3.4 Parallelism and Memory Resources

The available degree of parallelism, counted as a number of simultaneous computations of line 17 in Listing 2, is determined by the number of compute units N_c . Every one of these compute units must read and write an element of C from fast memory *every cycle*. This implies a minimum number of *parallel* fast memory accesses

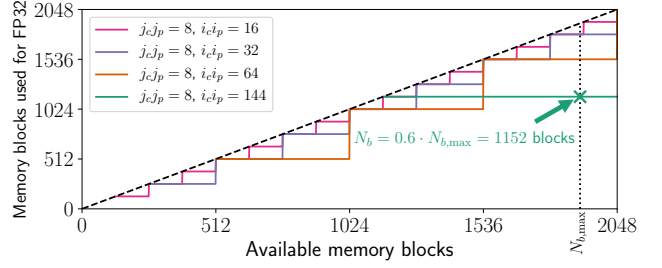


Figure 3: Utilization of memory blocks with memory tile size. For $i_c j_c = 8$ and $i_p j_p = 144$, we can utilize $60.4\% \cdot N_{b,\max}$.

that must be supported in the architecture. Memory blocks expose a limited access width w_b (measured in bits), which constrains how much data can be read from/written to them in a single cycle. We can thus infer a minimum number of memory blocks necessary to serve all compute units in parallel, given by:

$$N_{b,\min} = x_p y_p \cdot \left\lceil \frac{w_c \cdot x_c y_c}{w_b} \right\rceil, \quad (8)$$

where w_c is the width of the data type in bits, and $x_c y_c$ denotes the granularity of a processing element. Because all $x_c y_c$ accesses within a processing element happen in parallel, accesses to fast memory can be coalesced into long words of size $w_c \cdot x_c y_c$ bits. For cases where w_b is not a multiple of w_c , the ceiling in Eq. 8 may be significant for the resulting $N_{b,\min}$. When instantiating fast memory to implement the tiling strategy, Eq. 8 defines the minimum “step size” we can take when increasing the tile sizes.

Within a full memory tile, each updated value $C[i, j]$ is reused after all $x_{\text{tot}} \cdot y_{\text{tot}}$ elements in a single memory tile are evaluated, and computation proceeds to the next iteration of the k -loop (line 4 in Listing 2). Given the intrinsic size of each memory block s_b , we can thus perform s_b iterations of the compute tile before a single batch of $N_{b,\min}$ allocated memory blocks has been filled up. If the total number of memory blocks $N_{b,\max} \geq 2N_{b,\min}$, i.e., the number of blocks required to support the parallel access requirements is less than the total number of blocks available, we can perform additional $\left\lfloor \frac{N_b}{N_{b,\min}} \right\rfloor$ iterations of the block tile, using all available memory blocks (up to the additive factor of $N_b \bmod N_{b,\min}$). However, for large available parallelism N_c , this additive factor may play a significant role, resulting in a part of available on-chip memory not being used. This effect is depicted in Fig. 3 for different values of N_c for the case of single precision floating point (FP32) in Xilinx BRAM blocks, where $s_b = 1024$ and $w_b = 36$ bit. The total number of memory blocks that can be efficiently used, without sacrificing the compute performance and load balancing constraints, is then:

$$N_b = \left\lfloor \frac{N_{b,\max}}{N_{b,\min}} \right\rfloor N_{b,\min}. \quad (9)$$

In the worst case, this implies that only $N_{b,\max}/2 + 1$ memory blocks are used. In the best case, $N_{b,\max}$ is a multiple of $N_{b,\min}$, and all memory block resources can be utilized. When $N_c > N_{b,\max}/2$, the memory tile collapses to a single block tile, and the total memory block usage is equal to Eq. 8.

4 HARDWARE MAPPING

With the goals for compute performance and I/O optimality set by the model, we now describe a mapping to a concrete hardware implementation.

4.1 Layout of Processing Elements

For Eq. 2 to hold, all N_p PEs must run at full throughput execution of the kernel, computing distinct contributions to the output tile. In terms of the proposed tiling scheme, we must evaluate a full compute tile t (second layer in Fig. 2) every cycle, which consists of $x_p \cdot y_p$ PE tiles (first layer in Fig. 2), each performing $x_c \cdot y_c$ calculations in parallel, contributing a total of N_c multiplications and additions towards the outer product currently being computed. Assuming that N_p elements of A and a full row of y_{tot} elements of B have been prefetched, we must – for each of the x_p rows of the first layer in Fig. 2 – propagate x_c values to all y_p horizontal PEs, and equivalently for columns of B . If this was broadcasted directly, it would lead to a total fan-out of $x_p \cdot y_p$ for both inputs.

Rather than broadcasting, we can exploit the regular grid structure, letting each column forward values of A , and each row forward values of B , in a pipelined fashion. Such an architecture is sometimes referred to as a *systolic array*, and is illustrated in Fig. 4. In this setup, each processing element has three inputs and three outputs (for A , B , and C), and dedicated Feed A and Feed B modules send prefetched contributions to the outer product at the left and top edges of the grid, while Store C consumes the output values of C written back by the PEs. The number of inter-module connections for this design is $3x_p y_p$, but more importantly, the fan-out of all modules is now constant, with 6 data buses per PE. Each PE is responsible for fully evaluating $x_{tot} y_{tot} / N_p$ elements of the output tile of C . The elements of each PE tile in Fig. 2 are stored contiguously (the first layer), but all subsequent layers are not – only the compute tile as a whole in contiguous in C . Final results must thus be written back in an interleaved manner to achieve contiguous writes back to C .

Collapsing to a 1D array. Although the 2D array of PEs is intuitive for performing matrix multiplication, it requires a grid-like structure to be routed on the chip. While this solves the issue of individual fan-out – and may indeed be sufficient for monolithic devices with all logic arranged in a rectangular structure – we wish to map efficiently onto general interconnects, including non-uniform and hierarchical structures, as well as multiple-chiplet FPGAs (or, potentially, multiple FPGAs). To achieve this, we can optionally collapse the 2D array of PEs into a 1D array by fixing $y_p = 1$, resulting in $N_p = x_p$ PEs connected in sequence. Since this results in a long, narrow compute tile, we additionally fix $x_c = 1$, relying on y_c to regulate the PE granularity. Forming narrow compute tiles is possible without violating Eq. 7, as long as x_{tot} and y_{tot} are kept identical (or as similar as possible), which we can achieve by regulating the outer block and tiling layers (the memory and block tile layers in Fig. 2).

Double buffering. Since each PE in the 1D array now computes one or more full rows of the compute tile, we can buffer values of A in internal registers, rather than from external modules. These can be propagated through the array from the first element to the last, then kept in local registers and applied to values of B that

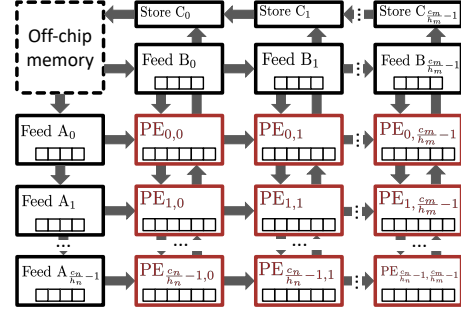


Figure 4: Compute arranged in a 2D grid.

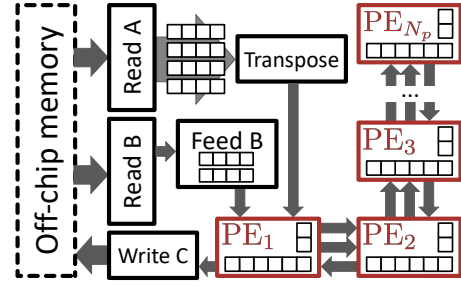


Figure 5: Module layout of final kernel architecture.

are streamed through the array from a buffer before the first PE. Since the number of PEs in the final design is large, we overlap the propagation of new values of A with the computation of the outer product contribution using the previous values of A , by using *double buffering*, requiring two registers per PE, i.e., $2N_p$ total registers across the design.

By absorbing the buffering of A into the PEs, we have reduced the architecture to a simple chain of width 1, reducing the total number of inter-module connections for the compute to $3N_p$, with 3 buses connecting each PE transition. When crossing interconnects with long timing delays or limited width, such as connections between chiplets, this means that only 3 buses must cross the gap, instead of a number proportional to the circumference of the number of compute units within a single chiplet, as was the case for the 2D design. As a situational downside, this increases the number of pipeline stages in the architecture when maximizing compute, which means that the number of compute tiles must be larger than the number of PEs, i.e., $y_t x_t \geq N_p$. This extra constraint is easily met when minimizing I/O, as the block tile size is set to a multiple of s_b (see Sec. 3.3), which in practice is higher than the number of PEs, assuming that extreme cases like $x_c = y_c = 1$ are avoided for large N_c .

4.2 Handling Loop-carried Dependencies

Floating point accumulation is often not a native operation on FPGAs, which can introduce loop-carried dependencies on the accumulation variable. This issue is circumvented with our decomposition. Each outer product consists of $x_p x_m \cdot y_p y_m$ inner memory tiles. Because each tile reduces into a distinct location in fast memory, collisions are separated by $x_p x_m \cdot y_p y_m$ cycles, and thus do

not obstruct pipelining for practical memory tile sizes (i.e., where $x_p x_m \cdot y_p y_m$ is bigger than the accumulation latency).

For data types such as integers or fixed point numbers, or architectures that support (and benefit from) pipelined accumulation of floating point types, it is possible to make k the innermost loop, optionally tiling n and m further to improve efficiency of reads from off-chip memory. The hardware architecture for such a setup is largely the same as the architecture proposed here, but changes the memory access pattern.

4.3 Optimizing Column-wise Reads

In the outer product formulation, the A -matrix must be read in a column-wise fashion. For memory stored as row-major, this results in slow and wasteful reads from DDR memory (in a column-major setting, the same argument applies, but for B instead). For DDR4 memory, a minimum of 512 bits must be transferred to make up for the I/O clock multiplier, and much longer bursts are required to saturate DDR bandwidth in practice. To make up for this, we can perform on-the-fly transposition of A as part of the hardware design in an additional module, by reading wide vectors and pushing them to separate FIFOs of depth $\geq x_b x_m$, which are popped in transposed order when sent to the kernel (this module can be omitted in the implementation at configuration time if A is pre-transposed, or an additional such module is added if B is passed in transposed form).

4.4 Writing Back Results

Each final tile of C is stored across the chain of processing in a way that requires interleaving of results from different PEs when writing it back to memory. Values are propagated backwards through the PEs, and are written back to memory at the head of the chain, ensuring that only the first PE must be close to the memory modules accessing off-chip memory. In previous work, double buffering is often employed for draining results, at the significant cost of reducing the available fast memory from S to $S/2$ in Eq. 6, resulting in a reduction in the arithmetic intensity of $\sqrt{2}$. To achieve optimal fast memory usage, we can leave writing out results as a sequential stage performed after computing each memory tile. It takes nm/y_c cycles to write back values of C throughout kernel execution, compared to nmk/N_c cycles taken to perform the compute. When $k/N_c \gg 1$, i.e., the matrix is large compared to the degree of parallelism, this effect of draining memory tiles becomes negligible.

4.5 Final Module Layout

With the constraints and considerations accumulated above, we fix the final hardware architecture. The module layout is shown in Fig. 5, and consists of $4 + N_p$ modules. The Feed B module buffers the outer product row of B , whereas N_p values of A are kept in PE registers. The vast majority of fast memory is spent in buffering the output tile of C (see Sec. 3.2), which is partitioned across the PEs, with $\frac{x_{tot} \cdot y_{tot}}{N_p}$ elements stored in each. The Read A and Transpose modules are connected with a series of FIFOs, the number of which is determined by the desired memory efficiency in reading A from DRAM. In our provided implementation, PEs are connected in a 1D sequence, and can thus be routed across the FPGA in a “snake-like” fashion [25] to maximize resource utilization with minimum routing constraints introduced by the module interconnect.

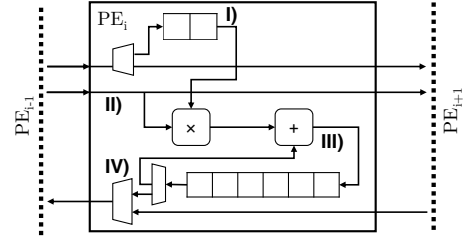


Figure 6: Architecture of a single PE.

The PE architecture is shown in Fig. 6. **I)** Each PE is responsible for storing a single double-buffered value of A . Values are loaded from memory and passed through the array, while the previous outer product is being computed. **II)** Values of B are streamed through the chain to be used at every PE. **III)** Every cycle accumulates into a different address of the output C until it repeats after $x_t x_b \cdot y_t y_b$ cycles. **IV)** When the outer tile has been computed, it is sent back through the PEs and written back at the memory interface.

5 EVALUATION

5.1 Parameter Selection

Using the performance model and hardware mapping considerations, parameters for kernel builds used to produce results are chosen in the following way, in order to maximize performance and minimize I/O based on available compute and memory resources, respectively:

- (1) The PE granularity is fixed at $x_c = 1$, and y_c is set as high as possible without impairing routing (determined empirically).
- (2) fN_c is maximized by scaling up parallelism $N_c = N_p \cdot y_c$ (we fixed $x_c = 1$) when the benefit is not eliminated by reduction in frequency, according to Eq. 2.
- (3) Memory tile sizes are maximized according to Eq. 9 to saturate on-chip memory resources.

For a given set of parameters, we build kernels in a *fully automated end-to-end fashion*, leveraging the abstractions provided by the high-level toolflow.

5.2 Code Complexity

The MMM kernel architecture used to produce the result in this work is implemented in Xilinx’ Vivado HLS tool with hlslib [8] extensions, and as of writing this paper, consists of 624 and 178 SLOC of C++ for kernel and header files, respectively. This is a generalized implementation, and includes variations to support transposed/non-transposed input matrices, variable/fixed matrix sizes, and different configurations of memory bus widths. Additionally, the operations performed by compute units can be specified, e.g., to compute the distance product by replacing multiply and add with add and minimum. The full source code is available on github under an open source license (see footnote on first page).

5.3 Experimental Setup

We evaluate our implementation on a Xilinx VCU1525 accelerator board, which hosts an Virtex UltraScale+ XCVU9P FPGA. The board

has four DDR4 DIMMs, but due to the minimal amount of I/O required by our design, a single DIMM is sufficient to saturate the kernel. The chip is partitioned into three chiplets, that have a total of 1,033,608 LUTs, 2,174,048 *flip-flops* (FFs), 6834 DSPs, and 1906 BRAMs available to our kernels. This corresponds to 87%, 92%, 99.9%, and 90% of data sheet numbers, respectively, where the remaining space is occupied by the provided shell.

Our kernels are written in Vivado HLS targeting the `xilinx:vcu1525:dynamic:5.1` platform of the SDAccel 2018.2 framework, and `-O3` is used for compilation. We target 200 MHz in Vivado HLS and SDAccel, although this is often reduced by the tool in practice due to congestion in the routed design for large designs, in particular paths that cross between chiplets on the FPGA (see Sec. 2). Because of the high resource utilization, each kernel build takes between 8 and 24 hours to finish successfully, or between 4 and 24 hours to fail placement or routing.

On the Virtex UltraScale+ architecture, floating point operations are not supported natively, and must be implemented using a combination of DSPs and general purpose logic provided by the toolflow. The resource vector `r` thus has the dimensions LUTs, FFs, and DSPs. The Vivado HLS toolflow allows choosing from multiple floating point implementations, that provide different trade-offs between LUT/FF and DSP usage. In general, we found that choosing implementations of floating point addition that does not use DSPs yielded better results, as DSPs replace little general purpose logic for this operation, and are thus better spent on instantiating more multiplications.

Memory blocks are implemented in terms of BRAM, where each block has a maximum port width of 36 bit of simultaneous read and write access to 18 kbit of storage. For wider data types, multiple BRAMs are coalesced. Each BRAM can store $s_{b,36\text{ bit}} = 1024$ elements in 36 bit configuration (e.g., FP32), $s_{b,18\text{ bit}} = 2048$ elements in 18 bit configuration (e.g., FP16), and $s_{b,72\text{ bit}} = 512$ elements in 72 bit configuration (e.g., FP64). For this work, we do not consider UltraRAM, which is a different class of memory blocks on the UltraScale+ architecture, but note that these can be exploited with the same arguments as for BRAM (according to the principles in Sec. 3.3). For benchmarked kernels we report the compute and memory utilization in terms of the hardware constraints, with the primary bottleneck for I/O being BRAM, and the bottleneck for performance varying between LUTs and DSPs, depending on the data type.

5.4 Results

We evaluate the computational performance and communication behavior of our approach by constructing kernels within varying logic and storage budgets, based on our C++ reference implementation. To explore the scaling behavior with increased parallelism, we measure strong scaling when increasing the number of PEs, shown in Fig. 7, by increasing N_c for $16384 \times 16384 \times 16384$ matrices. We report the median across 20 runs, and omit confidence intervals, as all kernels behaved deterministically, making errors negligible. To measure power efficiency, we sample the direct current power draw of the PSU in the host machine, then determine the FPGA power consumption by computing the difference between the machine at idle with no FPGA plugged in, and the FPGA plugged in

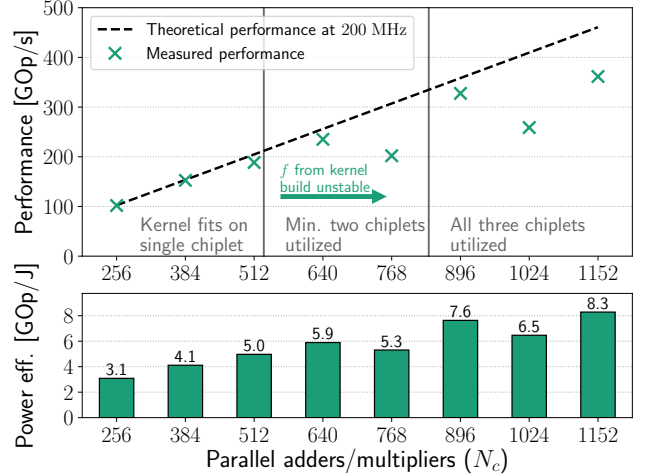


Figure 7: Strong scaling for single precision floating point, $n=m=k=16384$ matrices.

while running the kernel. This method includes power drawn by the full VCU1525 evaluation board, including the integrated fan. The kernels compile to maximum performance given by each configurations at 200 MHz until the first chiplet/SLR crossing, at which point the clock frequency starts degrading. This indicates that the chiplet crossings are the main contributor to long timing paths in the design that bottleneck the frequency.

Tab. 2 shows the configuration parameters and measured results for the highest performing kernel built using our architecture for half, single and double precision floating point types, as well as 8-bit, 16-bit, and 32-bit unsigned integer types. Timing issues from placement and routing are the main bottleneck for all kernels, as the frequency for the final routed designs start to be unstable beyond 33% resource usage, when the number of chiplet crossings becomes significant (shown in Fig. 7). When resource usage exceeds 80–90%, kernels fail to route or meet timing entirely. Due to the large step size in BRAM consumption for large compute tiles when targeting peak performance (see Sec. 3.3), some kernels consume less BRAM than what would otherwise be feasible to route, as increasing the memory tile by another stage of $N_{b,\text{min}}$ would exceed $N_{b,\text{max}}$.

In contrast to previous implementations, we achieve optimal usage of the on-chip memory by separating the drain phase of writing out results from the compute phase. This requires the number of computations performed per memory tile to be significantly larger than the number of cycles taken to write the tile out to memory (see Sec. 4.4). This effect is shown in Fig. 8 for small N_c (left) and large N_c (right). For large N_c , the time spent in draining the result is significant for small matrices. In either scenario, optimal computational efficiency is approached for large matrices, when there is sufficient work to do between draining each result tile.

Fig. 9 demonstrates the reduction in communication volume with increasing values of the outer I/O tiles (i.e., $x_t x_b \cdot y_t y_b$). We plot the arithmetic intensity, corresponding to $2 \times$ the computational intensity in Eq. 3 (1 addition and 1 multiplication), and verify that the communication volume reported by the runtime is verified to match the analytical value computed with Eq. 6. We also report the

Data type	x_p	y_c	x_{tot}	y_{tot}	Frequency	Performance	Power eff.	Arithm. int.	LUTs	FFs	DSPs	BRAM
FP16	112	16	1904	1920	171.3 MHz	606 GOp/s	15.1 GOp/J	956 Op/Byte	53%	24%	70%	90%
FP32	192	8	960	1632	145.7 MHz	409 GOp/s	10.9 GOp/J	302 Op/Byte	81%	46%	48%	80%
FP64	96	4	864	864	181.2 MHz	132 GOp/s	3.13 GOp/J	108 Op/Byte	38%	28%	80%	82%
uint8	132	32	1980	2176	186.5 MHz	1544 GOp/s	48.0 GOp/J	2073 Op/Byte	15%	8%	83%	51%
uint16	210	16	1680	2048	190.0 MHz	1217 GOp/s	33.1 GOp/J	923 Op/Byte	20%	11%	69%	88%
uint32	202	8	1212	1360	160.6 MHz	505 GOp/s	13.8 GOp/J	320 Op/Byte	58%	11%	84%	86%

Table 2: Highest performing kernels built for each data type.

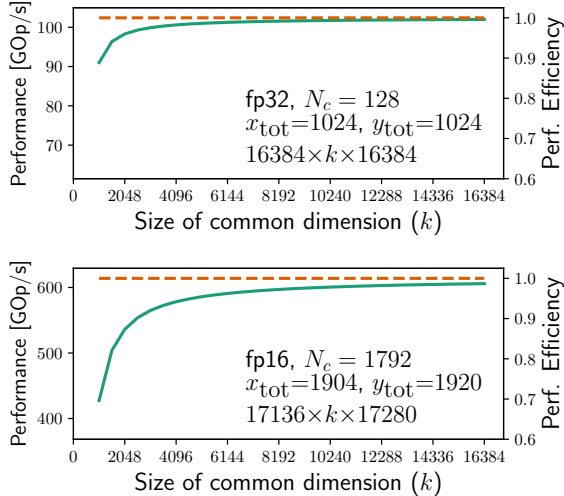


Figure 8: Fraction of maximum compute throughput for varying matrix size.

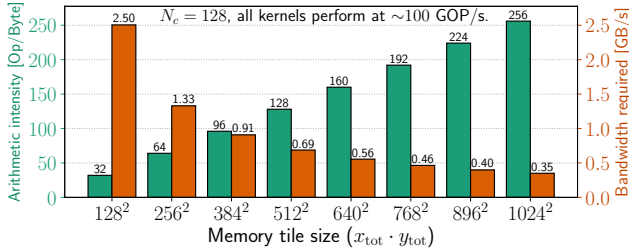


Figure 9: FP32 arithmetic intensity with memory tile size.

average bandwidth requirement needed to run each kernel (in practice, the bandwidth consumption is not constant during runtime, as memory accesses are done as bursts each time the row and column for a new outer product is loaded). There is a slight performance benefit from increasing memory tile size, as larger tiles increase the ratio of cycles spent in the compute phase to cycles spent writing back results, approaching perfect compute/DSP efficiency for large matrices. For the largest tile size, the kernel consumes 350 MB/s at 100 GOp/s, which corresponds to $\frac{350}{19200} = 1.8\%$ of the maximum bandwidth of a single DDR4 module. Even at the highest measured single precision performance (Tab. 2) of 409 GOp/s, the kernel requires 1.35 GB/s. This brings the I/O of matrix multiplication down to a level where nearly the full bandwidth is left available.

6 RELATED WORK

Much of previous work focuses on the low level implementation for performance [22], explores high-level optimizations [12], or implements MMM in the context of neural networks [16, 27]. To the best of our knowledge, this is the first work to minimize I/O of matrix multiplication on FPGA *in terms of hardware constants*, and the first work to open source our implementation to benefit of the community. We relate this paper to the most relevant works below.

Tab. 3 shows a hybrid qualitative/quantitative comparison to previously published MMM implementations on FPGA. Cells are left empty when numbers are not reported by the authors, or when the given operation is not supported. As our work is the only open source implementation, we are unable to execute kernels from other works on the same FPGA, and resort to comparing the performance reported in papers for the respective benchmarked FPGA. These FPGAs thus vary widely in vendor, technology and architecture.

Zhuo and Prasanna [35] discuss two matrix multiplication implementations on FPGA, and include routing in their considerations, and support multiple floating point precisions. The authors suggest two algorithms, where both require a number of PEs proportional to the matrix size. While these only require loading each matrix once, they do not support matrices of arbitrary size, and thus do not scale without additional CPU orchestration.

Dou et al. [13] design a linear array of processing elements, implementing 64-bit floating point matrix multiplication – no support is offered for other data types, as the work emphasizes the low-level implementation of the floating point units. The authors derive the required off-chip bandwidth and buffer space required to achieve peak performance on the target device, but do not model or optimize I/O in terms of their buffer space usage, and do not report their tile sizes or how they were chosen. Furthermore, the authors double-buffer the output tile, reducing the maximum achievable computational intensity by a factor $\sqrt{2}$ (see Sec. 4.4).

A customizable matrix multiplication implementation for deep neural network applications on the Intel HARPv2 hybrid CPU/FPGA platform is presented by Moss et al. [27], targeting single precision floating point (FP32), and fixed point/integer types. The authors exploit native floating point DSPs on an Arria 10 device to perform accumulation, and do not consider data types that cannot be natively accumulated on their chip, such as half or double precision. The I/O characteristics of the approach is not reported quantitatively. Wu et al. [32] present a highly specialized architecture for maximizing DSP usage and frequency of 16 bit integer matrix multiplication for DNN acceleration on two Xilinx Ultra-Scale chips, showing how peak DSP utilization and frequency can be reached, at the expense of generality, as the approach relies on

	Year	Device	% Logic util.	Freq. [MHz]	Perf. FP16 [GOp/s]	Perf. FP32 [GOp/s]	Perf. FP64 [GOp/s]	Energy eff. FP32 [GOp/J]	Multiple data types	Lang. (Portable)	Open source	I/O model
Zhuo [35]	2004	Virtex-II Pro	98	128	-	2	2	-	🔒	HDL (🔒)	🔒	🔒
Dou [13]	2005	Virtex-II Pro	99	177	-	-	39	-	🔒	HDL (🔒)	🔒	🔒
Kumar [23]	2009	Virtex-5	61	373 [†]	-	-	30 [†]	-	🔒	HDL (🔒)	🔒	👍
Jovanović [22]	2012	Virtex-6	100	403	-	203	-	-	🔒	HDL (🔒)	🔒	🔒
D'Hollander [12]	2016	Zynq-7000	99	100	-	5	-	-	🔒	HLS (👍)	🔒	🔒
Guan [16]	2017	Stratix V	95	150	-	100	-	2.92	👍	HDL/HLS (🔒)	🔒	🔒
Moss [27]	2018	HARPV2	99	313	-	800	-	22.0	👍	HDL (🔒)	🔒	🔒
This work	2019	VCU1525	69–90	146–190	606	409	122	10.9	👍	HLS (👍)	👍	👍

Table 3: Comparison to previous FPGA implementations. [†]Simulation only.

low-level details of the chips’ architecture, and as no other data types are supported.

Kumar et al. [23] provide an analysis of the trade-off between I/O bandwidth and on-chip memory for their implementation of 64-bit matrix multiplication. The authors arrive at a square output tile when deriving the constraints for overlapping I/O, although the derived computational intensity is reduced by a factor $\sqrt{2}$ as above from double buffering. In our model, the fast memory utilization is captured explicitly, and is maximized in terms of on-chip memory characteristics of the target FPGA, allowing tile sizes that optimize both computational performance and computational intensity to be derived directly. Lin and Leong [26] model sparse MMM, with dense MMM as a special case, and project that even dense matrix multiplication may become I/O bound in future FPGA generations. Our model guides how to maximize utilization in terms of available on-chip memory to mitigate this, by capturing their characteristics in the tiling hierarchy.

Finally, the works above were implemented in hardware description languages, and *do not disclose the source code allowing their findings to be reproduced or ported to other FPGAs*. For the results presented here, we provide a high-level open source implementation, to encourage reusability and portability of FPGA codes.

Designing I/O minimizing algorithms has been an active field of research for more than 40 years. Starting with register allocation problems [5], through single processor, two-level memory system [21], distributed systems with fixed [20] and variable memory size [29]. Although most of the work focus on linear algebra [14, 20, 29] due to its regular access pattern and powerful techniques like polyhedral modeling, the implication of these optimizations far exceeds this domain. Gholami et al. [15] studied model and data parallelism of DNN in the context of minimizing I/O for matrix multiplication routines. Demmel and Dinh [10] analyzed I/O optimal tiling strategies for convolutional layers of NN.

7 CONCLUSION

We present a high-performance, open source, flexible, portable, and scalable matrix-matrix multiplication implementation on FPGA, which simultaneously maximizes performance and minimizes off-chip data movement. By starting from a general model for computation, I/O, and resource consumption, we create a hardware architecture that is optimized to the resources available on a target device, and is thus not tied to specific hardware. We evaluate our implementation on a wide variety of data types and configurations, showing 409 GOp/s 32-bit floating point performance, and

1.5 Top/s 8-bit integer performance, utilizing >80% of hardware resources. We show that our model-driven I/O optimal design is robust and high-performant in practice, yielding better or comparable performance to HDL-based implementations, and conserving bandwidth to off-chip memory, while being easy to configure, maintain and modify through the high-level HLS source code.

ACKNOWLEDGMENTS

We thank Xilinx for generous donations of software and hardware. This project has received funding from the European Research Council (ERC) under the European Union’s Horizon 2020 programme (grant agreement DAPP, No. 678880).

REFERENCES

- [1] Alok Aggarwal and S. Vitter. 1988. The Input/Output Complexity of Sorting and Related Problems. *Commun. ACM* 31, 9 (Sept. 1988).
- [2] Edward Anderson, Zhaojun Bai, Christian Bischof, L Susan Blackford, James Demmel, Jack Dongarra, Jeremy Du Croz, Anne Greenbaum, Sven Hammarling, Alan McKeeney, et al. 1999. *LAPACK Users’ guide*. SIAM.
- [3] Michael Anderson, Grey Ballard, James Demmel, and Kurt Keutzer. 2011. Communication-avoiding QR decomposition for GPUs. In *Parallel & Distributed Processing Symposium (IPDPS), 2011 IEEE International*. IEEE, 48–58.
- [4] Tal Ben-Nun and Torsten Hoefler. 2019. Demystifying parallel and distributed deep learning: An in-depth concurrency analysis. *ACM Computing Surveys (CSUR)* 52, 4 (2019), 65.
- [5] Gregory J. Chaitin, Marc A. Auslander, Ashok K. Chandra, John Cocke, Martin E. Hopkins, and Peter W. Markstein. 1981. Register allocation via coloring. *Computer Languages* 6, 1 (1981), 47 – 57.
- [6] Michael Christ, James Demmel, Nicholas Knight, Thomas Scanlon, and Katherine Yelick. 2013. Communication lower bounds and optimal algorithms for programs that reference arrays—Part 1. *arXiv preprint arXiv:1308.0068* (2013).
- [7] Paolo D’Alberto and Alexandru Nicolau. 2008. Using recursion to boost ATLAS’s performance. In *High-Performance Computing*. Springer, 142–151.
- [8] Johannes de Fine Licht and Torsten Hoefler. 2019. hlslib: Software Engineering for Hardware Design. *arXiv preprint arXiv:1910.04436* (2019).
- [9] Mauro Del Ben et al. 2015. Enabling simulation at the fifth rung of DFT: Large scale RPA calculations with excellent time to solution. *Comp. Phys. Comm.* (2015).
- [10] James Demmel and Grace Dinh. 2018. Communication-Optimal Convolutional Neural Nets. *arXiv preprint arXiv:1802.06905* (2018).
- [11] James Demmel, David Eliahu, Armando Fox, Shoaib Kamil, Benjamin Lipshitz, Oded Schwartz, and Omer Spillinger. 2013. Communication-Optimal Parallel Recursive Rectangular Matrix Multiplication. In *Proceedings of the 2013 IEEE 27th International Symposium on Parallel and Distributed Processing (IPDPS ’13)*. 261–272.
- [12] Erik H. D’Hollander. 2017. High-Level Synthesis Optimization for Blocked Floating-Point Matrix Multiplication. *SIGARCH Comput. Archit. News* 44, 4 (Jan. 2017), 74–79. <https://doi.org/10.1145/3039902.3039916>
- [13] Yong Dou, S. Vassiliadis, G. K. Kuzmanov, and G. N. Gaydadjiev. 2005. 64-bit Floating-point FPGA Matrix Multiplication. In *Proceedings of the 2005 ACM/SIGDA 13th International Symposium on Field-programmable Gate Arrays (Monterey, California, USA) (FPGA ’05)*. ACM, New York, NY, USA, 86–95. <https://doi.org/10.1145/1046192.1046204>
- [14] G. A. Geist and E. Ng. 1990. Task Scheduling for Parallel Sparse Cholesky Factorization. *Int. J. Parallel Program.* 18, 4 (July 1990), 291–314. <https://doi.org/10.1007/BF01407861>

- [15] Amir Gholami, Ariful Azad, Peter Jin, Kurt Keutzer, and Aydin Buluc. 2017. Integrated model, batch and domain parallelism in training neural networks. *arXiv preprint arXiv:1712.04432* (2017).
- [16] Y. Guan, H. Liang, N. Xu, W. Wang, S. Shi, X. Chen, G. Sun, W. Zhang, and J. Cong. 2017. FP-DNN: An Automated Framework for Mapping Deep Neural Networks onto FPGAs with RTL-HLS Hybrid Templates. In *2017 IEEE 25th Annual International Symposium on Field-Programmable Custom Computing Machines (FCCM)*. 152–159. <https://doi.org/10.1109/FCCM.2017.25>
- [17] Azzam Haidar, Stanimire Tomov, Jack Dongarra, and Nicholas J Higham. 2018. Harnessing GPU tensor cores for fast FP16 arithmetic to speed up mixed-precision iterative refinement solvers. In *Proceedings of the International Conference for High Performance Computing, Networking, Storage, and Analysis*. IEEE Press, 47.
- [18] Intel. 2007. *Intel Math Kernel Library (MKL)*. <https://software.intel.com/en-us/mkl>
- [19] Dror Irony et al. 2004. Communication Lower Bounds for Distributed-memory Matrix Multiplication. *JPDC* (2004).
- [20] Dror Irony, Sivan Toledo, and Alexander Tiskin. 2004. Communication lower bounds for distributed-memory matrix multiplication. *J. Parallel and Distrib. Comput.* 64, 9 (2004), 1017–1026.
- [21] Hong Jia-Wei and Hsiang-Tsung Kung. 1981. I/O complexity: The red-blue pebble game. In *Proceedings of the thirteenth annual ACM symposium on Theory of computing*. ACM, 326–333.
- [22] Zeljko Jovanović and V Milutinovic. 2012. FPGA accelerator for floating-point matrix multiplication. *IET Computers & Digital Techniques* 6, 4 (2012), 249–256.
- [23] V. B. Y. Kumar, S. Joshi, S. B. Patkar, and H. Narayanan. 2009. FPGA Based High Performance Double-Precision Matrix Multiplication. In *2009 22nd International Conference on VLSI Design*. 341–346. <https://doi.org/10.1109/VLSI.Design.2009.13>
- [24] Grzegorz Kwasniewski, Marko Kabić, Maciej Besta, Joost VandeVondele, Raffaele Solcà, and Torsten Hoefler. 2019. Red-Blue Pebbling Revisited: Near Optimal Parallel Matrix-Matrix Multiplication. In *Proceedings of the International Conference for High Performance Computing, Networking, Storage, and Analysis (Denver, Colorado) (SC '19)*.
- [25] Chris Lavin and Alireza Kaviani. 2018. RapidWright: Enabling custom crafted implementations for FPGAs. In *2018 IEEE 26th Annual International Symposium on Field-Programmable Custom Computing Machines (FCCM)*. IEEE, 133–140.
- [26] Colin Yu Lin, Hayden Kwok-Hay So, and Philip HW Leong. 2011. A model for matrix multiplication performance on FPGAs. In *2011 21st International Conference on Field Programmable Logic and Applications*. IEEE, 305–310.
- [27] Duncan J.M Moss, Srivatsan Krishnan, Eriko Nurvitadhi, Piotr Ratuszniak, Chris Johnson, Jaewoong Sim, Asit Mishra, Debbie Marr, Suchit Subhaschandra, and Philip H.W. Leong. 2018. A Customizable Matrix Multiplication Framework for the Intel HARPv2 Xeon+FPGA Platform: A Deep Learning Case Study. In *Proceedings of the 2018 ACM/SIGDA International Symposium on Field-Programmable Gate Arrays (Monterey, California, USA) (FPGA '18)*. ACM, New York, NY, USA, 107–116. <https://doi.org/10.1145/3174243.3174258>
- [28] Michele Squizzato and Francesco Silvestri. 2013. Communication Lower Bounds for Distributed-Memory Computations. *arXiv preprint arXiv:1307.1805* (2013). [arXiv:1307.1805](https://arxiv.org/abs/1307.1805)
- [29] Edgar Solomonik and James Demmel. 2011. Communication-Optimal Parallel 2.5D Matrix Multiplication and LU Factorization Algorithms. In *Euro-Par 2011 Parallel Processing*, Emmanuel Jeannot, Raymond Namyst, and Jean Roman (Eds.). Springer Berlin Heidelberg, Berlin, Heidelberg, 90–109.
- [30] Volker Strassen. 1969. Gaussian Elimination is Not Optimal. *Numer. Math.* 13, 4 (Aug. 1969), 354–356. <https://doi.org/10.1007/BF02165411>
- [31] Vincent Vanhoucke, Andrew Senior, and Mark Z. Mao. 2011. Improving the speed of neural networks on CPUs. In *Proc. Deep Learning and Unsupervised Feature Learning NIPS Workshop*, Vol. 1. Citeseer.
- [32] Ephrem Wu, Xiaoqian Zhang, David Berman, and Inkeun Cho. 2017. A high-throughput reconfigurable processing array for neural networks. In *2017 27th International Conference on Field Programmable Logic and Applications (FPL)*. IEEE.
- [33] Wm. A. Wulf and Sally A. McKee. 1995. Hitting the Memory Wall: Implications of the Obvious. *SIGARCH Comput. Archit. News* 23, 1 (March 1995), 20–24. <https://doi.org/10.1145/216585.216588>
- [34] Hao Zhou and Jingling Xue. 2016. A Compiler Approach for Exploiting Partial SIMD Parallelism. *ACM Trans. Archit. Code Optim.* 13, 1, Article 11 (March 2016), 26 pages. <https://doi.org/10.1145/2886101>
- [35] L. Zhuo and V. K. Prasanna. 2004. Scalable and modular algorithms for floating-point matrix multiplication on FPGAs. In *18th International Parallel and Distributed Processing Symposium, 2004. Proceedings.* 92–. <https://doi.org/10.1109/IPDPS.2004.1303036>